IJE TRANSACTIONS A: Basics Vol. 39, No. 10, (October 2026) 2509-2520

International Journal of Engineering

Journal Homepage: www.ije.ir

A Comparative Study of Laminar and Turbulent Flow in Ribbed Wavy Channels: Effects of Rib Height, Angle, and Density

A. H. Ghalta[a,b], M. Farhadi*[b]

[a] Department of Refrigeration and Air Conditioning Engineering Technologies, College of Engineering Technologies, University of Hilla, Hilla, Iraq
[b] Faculty of Mechanical Engineering, Babol Noshirvani University of Technology, Babol, I. R. of Iran

PAPER INFO

Paper history:
Received 23 August 2025
Received in revised form 15 September 2025
Accepted 25 October 2025

Keywords:
Wavy Channel
Ribbed Surfaces
Heat Transfer Enhancement
Erformance Evaluation Criterion (PEC)

ABSTRACT

This study investigates the thermal–hydraulic performance of wavy channels equipped with transverse ribs, addressing the need for optimized heat transfer solutions in compact heat exchangers, where the combined effects of rib geometry and flow regime remain insufficiently explored. The objective is to evaluate how rib inclination angle, height, and count influence heat transfer enhancement and overall efficiency under both laminar (Re = 500) and turbulent (Re = 5000) flow conditions. Three-dimensional numerical simulations were performed using ANSYS Fluent to analyze heat transfer characteristics, frictional losses, and the performance evaluation criterion (PEC). The results show that transverse ribs significantly enhance heat transfer by promoting flow separation and vortex formation. In laminar flow, Nusselt numbers increased by up to ~50% compared to smooth channels, with optimal PEC values achieved at moderate rib heights (h/H = 0.2–0.4), rib angles of 45°–60°, and low rib counts (N = 1–2). In turbulent flow, heat transfer enhancement was more pronounced (Nusselt numbers ~56–58), although increased friction led to PEC values below unity in most cases. Novel trade-offs were identified that balance thermal performance and efficiency, especially in laminar regimes. These findings contribute valuable design guidelines for the geometric optimization of ribbed wavy channels in different flow regimes.

doi: *10.5829/ije.2026.39.10a.13*

Graphical Abstract

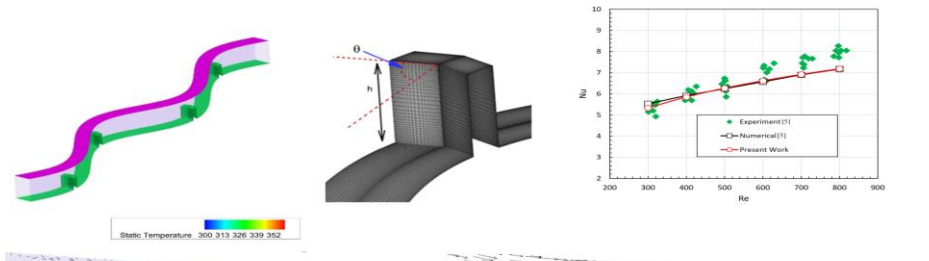

Flow Regime	Max Nu	Typical f (high h/H, N=4)	PEC Trend	Optimal Design
Laminar (Re=500)	~21–24	2.5–3.0	PEC ≈ 1 achievable at 45–60°, h/H=0.2–0.4, N=1–2	Moderate ribs, shallow angles
Turbulent Re=5000)	~56–58	1.5–1.8	PEC < 1 in most cases; best ≈ 0.9 at 45°, h/H≤0.2, N=1	Small ribs, low density

*Corresponding Author Email: mfarhadi@nit.ac.ir (M. Farhadi)

Please cite this article as: Ghalta AH, Farhadi M. A Comparative Study of Laminar and Turbulent Flow in Ribbed Wavy Channels: Effects of Rib Height, Angle, and Density. International Journal of Engineering, Transactions A: Basics. 2026;39(10):2509-20.

NOMENCLATURE

D_h	Hydrolic Diameter, $D_h = (2WH)/(H + W)$ *(m)*	T	Temperature (K)
h	Rib height (m)	$\mathrm{Re} = \rho D_h U/\mu$	Reynolds Number
H	Channel cross section height (m)	u_i, u_j	components of velocity (m/s)
W	Channel cross section width (m)	**Greek Symbols**	
h_{ave}	Mean heat transfer coefficient (W/m^2.K)	k	turbulence kinetic energy (m^2/s^2)
N	Number of Rib	μ	Dynamic viscosity (kg.m/s)
Nu	Nusselt number, $Nu = h_{ave} D_h/k_f$	ϴ	Rib angle (°, degree)
k_f	Conductivity of fluid (W/m.K)	α	Thermal diffusivity (m^2/s)
P	*Pressure (Pa)*	ν	Kinematic viscosity (m^2/s)
Pr	Prandtl number	ρ	Density (kg/m^3)
		ε	rate of dissipation (m^2/s^3)

1. INTRODUCTION

With the continuous miniaturization and increasing power density of electronic, optoelectronic, and photovoltaic (PV) devices, efficient thermal management has become a critical concern. Among the various strategies explored, microchannel heat sinks (MCHSs) have garnered significant attention due to their compact size, high surface-area-to-volume ratio, and superior heat dissipation capabilities. Over the past decade, researchers have extensively investigated enhancements in microchannel geometries, flow conditions, and working fluids to improve heat transfer performance while managing associated pressure drops (1-3). Early experimental studies, such as those by Sui et al. (4), revealed that wavy microchannels outperformed straight ones in terms of frictional flow and heat transfer characteristics. Building upon this, Zhou et al. (5) employed numerical simulations and response surface methodology to optimize sinusoidal wavy microchannel geometries, further validating their potential for compact heat sinks. Other geometric innovations have also shown promise; Kaewchoothong et al. (6) analyzed square cross-sectional obstacles and found that inclined and V-shaped obstacles enhanced heat transfer by up to 30%, depending on angle and configuration. Lin et al. (7) introduced a variable wavelength and amplitude wavy design that significantly reduced thermal resistance, while Rui and Kondo (8) highlighted the material and thermal advantages of triangular heat sinks over traditional rectangular fin arrays. Wang et al. (9) demonstrated the benefits of inclined rectangular obstacles in breaking thermal boundary layers and enhancing heat transfer. Meanwhile, Chai and Wang (10) analyzed five obstacle geometries in cross-sectional chambers and reported substantial reductions in thermal resistance and entropy generation. Bahiraei et al. (11) further improved performance using graphene-silver hybrid nanofluids in microchannels with ribs and sub-channels. Ghodavai and Hassan (12) studied the influence of obstacle height on local heat transfer, whereas Zhou et al. (13) compared left-right and top-bottom wavy designs, revealing Dean vortex formation as a critical mechanism in enhancing mixing and thermal performance. Li et al. (14) proposed a dual-layer heat sink with solid and porous obstacles that achieved low thermal resistance and uniform temperature distribution. Shuo-Wang et al. (15) expanded on this with a dual-layer design incorporating wavy channels and porous vertical obstacles, finding it more effective than straight channel configurations. Sheng and Wang et al. (16) investigated pulsating flow effects in fan-like microchannels using the lattice Boltzmann method, revealing that alternating flow structures improved mixing and heat transfer. Krishna et al. (17) emphasized the role of waviness in altering the transition Reynolds number and enhancing average Nusselt numbers. Ahmed et al. (18) applied a multi-level truncated fin design for natural convection cooling of PV modules, which reduced module temperature and increased power output. Khan and Karimi (19) and Al-Sabri et al. (20) further examined geometric modifications and nanofluid behavior in wavy microchannels.

Zhang et al. (21) compared dual-layer and straight channel MCHSs, confirming the thermal advantages of the dual-layer configuration. Khan et al. (22) validated the enhanced cooling of wavy and dual-wavy microchannels using nanofluids in laminar flows. Ghorbani et al. (23) identified that higher amplitude-to-wavelength ratios promoted turbulence and improved heat transfer in wavy designs. Shuo-Wang et al. (24) showed that symmetric wavy configurations generated four Dean vortices, improving heat transfer but increasing pressure drop. Okeb et al. (25) demonstrated that dimples and fillets significantly influenced the flow structure and thermal performance. Al-Naimat et al. (26) showed that zigzag channels reduced thermal resistance and pumping power. Halon et al. (27) explored two-phase boiling flows in restricted and unrestricted microchannels, revealing complex flow pattern dependencies. Finally, Fiu et al. (28) used machine learning and genetic algorithms to optimize wavy microchannel configurations for PV cooling, achieving high prediction accuracy and performance.

Recent studies have emphasized the pivotal role of geometry in optimizing microchannel heat sink (MCHS)

performance. Chen and Yaji (29) introduced a topology optimization framework using an Eulerian–Eulerian multiphase approach, achieving an 11.6% enhancement in heat transfer through geometrically optimized nanofluid channels. Nasiri Khamesloo and Domiri Ganji (30) proposed novel fractal MCHS designs with bottom and sidewall fins, revealing that sidewall fins improved Nusselt numbers by 28% and overall system performance by up to 6%. In another work, they showed that hybrid nanofluid flows in modified geometries further optimized thermal distribution (31). Zhu et al. (32) conducted a comparative assessment of rib shapes and cavity structures, concluding that geometric coupling significantly influences flow uniformity and heat transfer rates. Li et al. (33) investigated six fin shapes in MCHS designs, identifying those with minimal pressure drop and maximal thermal enhancement. Li and colleagues (34) also applied artificial neural networks and genetic algorithms to optimize pin-fin microchannels, leading to better temperature uniformity and thermal performance. Huo and Sun (35) developed a hierarchical embedded microchannel geometry for ultra-high flux SiC chip cooling, achieving exceptional thermal metrics using deionized water boiling. Chej et al. (36) modeled heat transfer in microfluidic sinks, showing how geometry-dependent temperature profiles impact flow behavior, especially at low Reynolds numbers. Al-Bahrani and co-authors (37) presented a topology-optimized fin architecture produced through additive manufacturing, enabling enhanced cooling via complex internal features. Jalilinasrabady and co-workers (38) reviewed inclined microchannel designs for microelectronics, highlighting their superior heat spreading potential. Dehkordi et al. (39) examined sinusoidal and Z-shaped patterns, concluding that increased surface contact via waviness improves convection. Mousavi and Rahimi (40) validated the effect of changing cross-sectional areas on flow acceleration and turbulence generation. Ghasemi and Arasteh (41) proposed a fluted-fin layout that enhanced thermal exchange in laminar regimes. Alimohammadi and Jamshidi (42) analyzed Y-shaped bifurcated microchannels, demonstrating superior distribution of flow and temperature control. Finally, Liu and Shi (43) introduced triangular lattice structures in the channel network, resulting in balanced heat spreading and reduced hotspots.

Despite the extensive literature on heat transfer enhancement, a comprehensive understanding of the combined effects of wavy channel geometries and internal obstacles—particularly V-shaped ribs—remains limited. To the best of our knowledge, there are no systematic studies investigating the influence of V-shaped ribs in wavy microchannels under both laminar and turbulent flow conditions. This study addresses this gap by numerically analyzing a novel ribbed wavy microchannel heat sink with axially aligned V-shaped ribs. Parametric investigations are performed for both laminar (Re = 500) and turbulent (Re = 5000) flow regimes, focusing on the effects of rib height-to-channel height ratio (h/H), rib angle (V-opening angle), and rib number (density) on Nusselt number, friction factor, thermal resistance, and the performance evaluation criterion (PEC).

2. GOVERNING EQUATION

The fluid flow and heat transfer in a three-dimensional domain under steady-state conditions, assuming an incompressible fluid with constant thermophysical properties, are governed by the following set of partial differential equations for laminar and turbulent flows:
Continuty equation:

$$\frac{\partial u_i}{\partial x_i} = 0 \tag{1}$$

Momentum equation:

$$u_j \frac{\partial u_i}{\partial x_j} = -\frac{1}{\rho}\frac{\partial P}{\partial x_i} + \nu \frac{\partial^2 u_i}{\partial x_j \partial x_j} \tag{2}$$

Energy equation:

$$u_j \frac{\partial T}{\partial x_j} = \alpha \frac{\partial^2 T}{\partial x_j \partial x_j} \tag{3}$$

The preceding equations are applicable to laminar flow regimes.

The time-averaging method in Reynolds-Averaged Navier-Stokes (RANS) equations is one of the common approaches in analyzing turbulent flows. In this method, by applying time-averaging to the Navier-Stokes equations, the Reynolds stress term emerges, which is caused by velocity fluctuations in turbulent flow. These additional stresses appear as indeterminate variables and require modeling to solve the equations.

One of the most common models for Reynolds stresses is the Eddy Viscosity Approach. In this method, Reynolds stresses are modeled similarly to molecular viscosity stresses, but instead of actual viscosity, an effective turbulent viscosity coefficient is introduced, which can simulate the effects of displacement and mixing caused by eddies. The resulting equations for the transfer of momentum and heat in turbulent flows are written as follows:

$$u_j \frac{\partial u_i}{\partial x_j} = -\frac{1}{\rho}\frac{\partial P}{\partial x_i} + (\nu + \nu_t)\frac{\partial^2 u_i}{\partial x_j \partial x_j} \tag{4}$$

$$u_j \frac{\partial T}{\partial x_j} = (\alpha + \alpha_t)\frac{\partial^2 T}{\partial x_j \partial x_j} \tag{5}$$

In these equations, the values of kinematic viscosity and the thermal diffusivity coefficient of turbulence are expressed as follows.

$$\nu_t = C_\mu \frac{k^2}{\varepsilon},\ \alpha_t = \frac{\nu_t}{\mathrm{Pr}_t} \tag{6}$$

The turbulence kinetic energy, k, and its rate of dissipation, ε, are obtained from the following transport equations:

$$\frac{\partial(ku_i)}{\partial x_i} = \frac{\partial}{\partial x_j}\left[(\nu + \frac{\nu_t}{\sigma_k})\frac{\partial k}{\partial x_j}\right] + P_k - \varepsilon + S_k \tag{7}$$

$$\frac{\partial(\varepsilon u_i)}{\partial x_i} = \frac{\partial}{\partial x_j}\left[(\nu + \frac{\nu_t}{\sigma_\varepsilon})\frac{\partial \varepsilon}{\partial x_j}\right] + C_{1\varepsilon}\frac{\varepsilon}{k}P_k - C_{1\varepsilon}\frac{\varepsilon^2}{k} + S_\varepsilon \tag{8}$$

The values of the constants in the equations are as follows.

$$C_\mu = 0.09, C_{1\varepsilon} = 1.44, C_{2\varepsilon} = 1.92, \sigma_k = 1.0, \sigma_\varepsilon = 1.3 \tag{9}$$

This study investigates fluid flow in a channel with a wavy cross-section and the presence of obstacles (Figure 1(a)). The channel geometry is rectangular with a height of 400 micrometers and a width of 216 micrometers, based on the research conducted by Ghorbani et. al. (24). The wavelength and wave amplitude are set at 2500 and 250 micrometers, respectively, as the baseline values for the channel's geometric structure. The obstacles are designed with V-shaped geometry, blocking between 0.1 to 0.5 of the channel's height and positioned along the flow path. The number of ribs (N) placed per wavelength of the wavy channel is limited to a maximum of four due to the geometric constraints of the wave structure. Ribs are positioned based on three distinct configurations: 1) only at the wave crests, 2) at both crests and troughs, and 3) at wave nodes with a 45° phase shift. These locations are physically meaningful and evenly distributed along the wave profile. As a result, placing more than four ribs within one wavelength would lead to overlapping or unrealistic rib positioning. Therefore, N= 1, 2, and 4 were selected as the practical and representative cases for analysis. To control computational volume and enhance the accuracy of the results, periodic boundary conditions have been applied. This approach ensures the independence of the results from the flow development length and improves computational efficiency. The rib angle is, in fact, half of the angle between the rib and its central axis (Figure 1(b)).

3. NUMERICAL METHOD

In this study, the commercial software ANSYS Fluent version 2021 was used. This program is based on the finite volume method, and the SIMPLE algorithm was used for pressure-velocity coupling. Non-linear terms in the momentum and energy equations were discretized using a second-order upwind scheme, and the residual value in the continuty equation was less than 10^{-3}, and in other equations up to 10^{-6}. The grid used was orthogonal and structured and had a higher concentration near the walls. In the turbulent flow, the y^+ value near the wall was reported to be less than 35. A sample of the generated grid is shown in Figure 1(b). The average difference between the grid numbers of the first and fourth is 4.51%, which has decreased to 0.4% with the further increase in number of grid points, particularly for the third and fourth grids. Considering the accuracy of the results and the savings in computational time and costs, the third grid points (with a size of 2,840,000 cells) was used in this study (Figure 2).

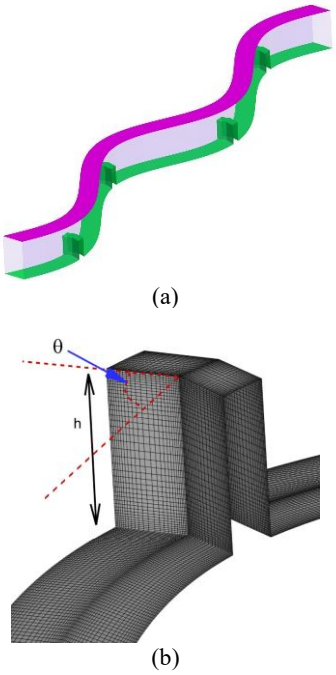

(a)

(b)

Figure 1. (a) Geometry of the problem; (b) A sample of grid points

4. RESULTS

To validate the numerical method employed, the results of Lu and Jiang (44) were simulated and compared. Their research includes experimental investigations of flow within a heated ribbed-surface channel. The present validation was conducted based on the channel configuration of 40 × 10 × 4 mm³, with a rib angle of 90 degrees and an inter-rib spacing of 4 mm. Results show that the present study predicted the experimental data with suitable accuracy in Nu number and friction factor

(Figure 3). The maximum error observed in the Nusselt number and friction factor were 5.8%, and 3%, respectively.

Subsequently, the experimental results of Sui et al. (5) concerning flow in a wavy microchannel were simulated (Figure 4). The simulation results demonstrated good agreement, with a maximum observed error of approximately 4%.

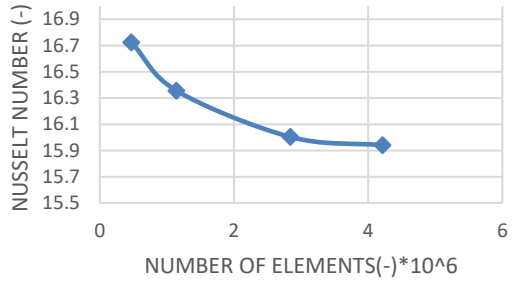

Figure 2. A grid independency

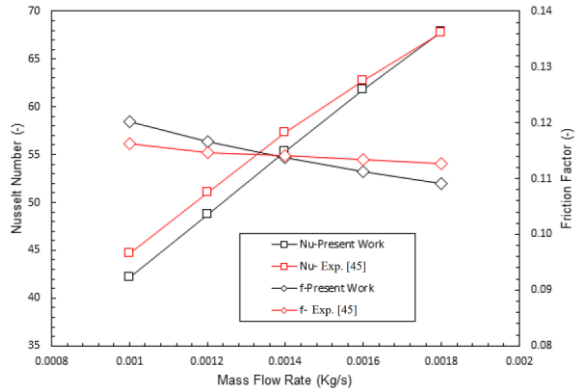

Figure 3. Comparison of the present numerical results with experimental data of Lu and Jiang (45) at turbulent flow

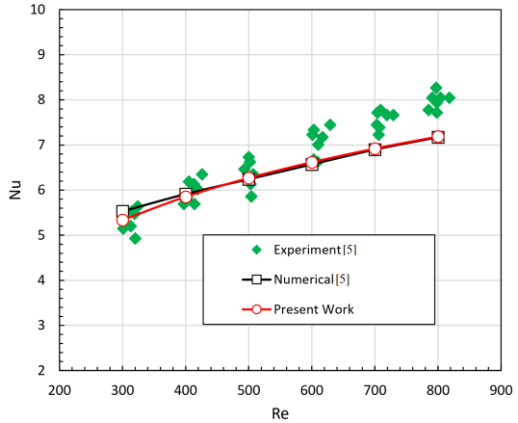

Figure 4. Comparison of the present numerical results with experimental and numerical data of Sui et al. (5) in a microchannel at laminar flow

4. 1. Heat Transfer and Friction Behavior Across Rib Angles (Laminar Flow) Figure 5 illustrates the variation of Nusselt number and friction factor as functions of the relative rib height *h/H* for rib inclination angles of 45°, 60°, 75°, and 90°, respectively, under laminar flow conditions (Re = 500). In all cases, three rib densities are considered: N = 1, 2, and 4. Across all angles, increasing the rib height consistently results in a higher Nusselt number, primarily due to improved boundary layer disruption and increased effective surface area. The most aggressive enhancement occurs for the 90° ribs, where the Nusselt number reaches values exceeding 24 for N = 4 at h/H=0.6. At 45°, the peak Nusselt number remains lower (around 21) but exhibits a more gradual increase with rib height. However, this thermal enhancement is accompanied by a substantial increase in friction factor, which becomes more pronounced at higher angles. At h/H=0.6 the friction factor reaches ~2.1 for 45°,~2.4 for 60°,~2.6 for 75° and ~3.0 for 90°. especially in the N = 4 configuration. This demonstrates that steeper rib angles, while thermally beneficial, impose a greater pressure drop penalty—particularly when combined with high rib density and height.

Figure 6 presents the three-dimensional streamlines and static temperature contours for a wavy channel with high rib height under (a) laminar and (b) turbulent flow conditions. The figure illustrates the complex vortex structures, recirculation zones, and heat transfer effects induced by ribbed geometry at elevated heights.

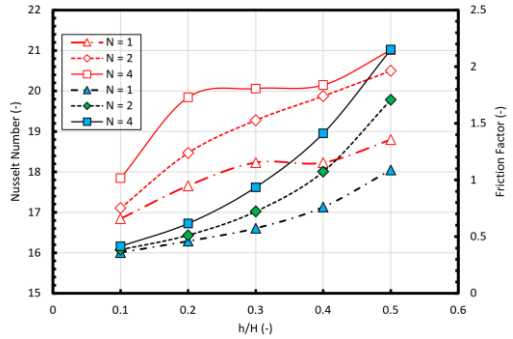

Angle = 45°

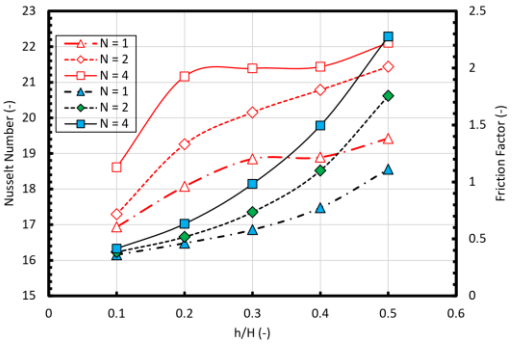

Angle = 60°

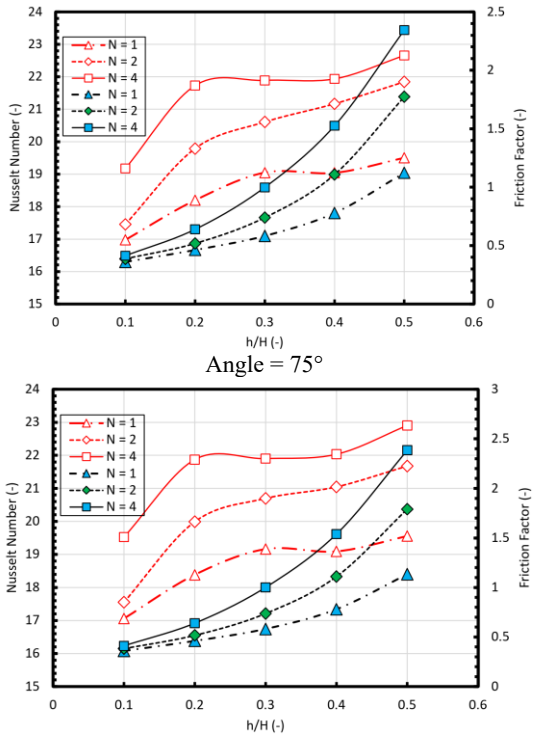

Figure 5. variation of Nusselt number and friction factor as functions of the relative rib height h/H for different rib inclination angles at laminar flow

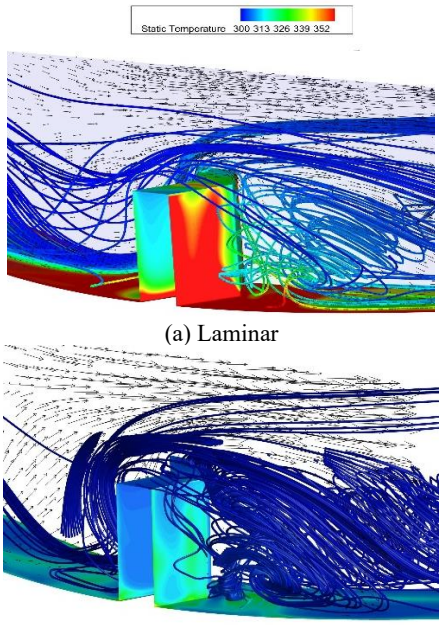

Figure 6. Three-dimensional streamlines and static temperature contours in a ribbed wavy channel with high rib height (h/H = 0.5) under (a) laminar and (b) turbulent flow conditions. Vortex formation, recirculation zones, and temperature gradients are shown to highlight the effect of rib geometry on flow structure and heat transfer

In the laminar flow case (Figure 6a), flow separation occurs immediately downstream of the ribs, generating stable and symmetric recirculating vortices in the cavity regions between ribs. As rib height increases from 0.1H to 0.2H, the size and strength of these vortices grow slightly, but the flow remains relatively ordered. However, a more significant change is observed when rib height reaches 0.5H: the vortices expand considerably, occupying nearly half the cavity height, and penetrate deeper into the core flow. This enhanced mixing contributes to stronger boundary layer disruption and improved heat transfer, as evidenced by the expanded isothermal layers near the rib walls.

In the turbulent flow case (Figure 6b), the increased rib height leads to an even more pronounced transformation. The flow becomes highly chaotic, with intense eddy formation, secondary flows, and complex vortex interactions in all three spatial directions. The high rib height forces the streamlines to bend sharply around obstacles, increasing the turbulent kinetic energy near the wall. The temperature contours show a thinner boundary layer and deeper thermal penetration into the core region, indicating stronger convective mixing than in the laminar case. Despite this improvement in heat transfer, such flow complexity also results in a higher friction factor and energy cost. Together, these visualizations demonstrate the critical role of rib height in shaping flow and thermal performance. While small ribs produce limited disruption, larger rib heights (e.g., h/H = 0.5) significantly enhance both vortex strength and thermal mixing, especially under turbulent conditions.

This expansion of the vortex zone intensifies flow mixing, boosts thermal energy exchange, and is consistent with the observed increase in the Nusselt number at higher rib heights. Nevertheless, the enlarged vortices also contribute to increased pressure drop, which must be balanced against the thermal gains in practical design. Figure 7 shows the Performance Evaluation Criterion (PEC) as a function of h/H for the same rib angles.

$$PEC = \frac{Nu / Nu_{Simple\ Wavy\ Channel}}{(f / f_{Simple\ Wavy\ Channel})^{1/3}} \quad (10)$$

A PEC value greater than 1 signifies a net thermal-hydraulic improvement. At 45°, PEC values approach unity for N = 1 and 2 at low rib heights ($h/H \leq 0.2$), but decline steadily beyond this point, dropping to ~0.7 for N = 4 at h/H=0.6. For 60°, 75°, and 90°, the PEC curves exhibit similar trends but decline more sharply, with the 90° configuration falling below 0.6 for high rib counts and heights. These findings indicate that while vertical or near-vertical ribs significantly enhance heat transfer, they do so at a disproportionate cost to pressure losses, reducing overall system efficiency.

Table 1 summarizes the optimal rib configurations for laminar flow conditions (Re = 500), based on a comprehensive evaluation of heat transfer (Nusselt number), frictional losses (friction factor), and overall thermal-hydraulic performance (PEC). For the single-rib configuration (N = 1), the optimal performance is achieved with rib angles between 45° and 60° and moderate rib heights in the range of $0.2 \leq h/H \leq 0.4$. This setup offers an excellent balance between enhanced heat transfer and low pressure drop, making it highly efficient for compact systems where pumping power must be minimized. The two-rib configuration (N = 2) performs best at a rib angle of 60° with slightly higher rib heights ($0.3 \leq h/H \leq 0.4$). This arrangement achieves a favorable compromise, offering improved heat transfer compared to N = 1, while maintaining manageable frictional penalties. It can be considered the most balanced choice among the tested geometries. In contrast, the four-rib configuration (N = 4) shows diminishing returns in performance, particularly at steeper angles (≥75°). Although it achieves higher Nusselt numbers, the associated pressure losses become dominant, especially at rib heights above 0.2H. Therefore, for high-density ribbing, the design must be restricted to low rib heights ($h/H \leq 0.2$) and shallower angles to avoid excessive flow resistance.

4. 2. Turbulent Flow Results (Re = 5000)

Figures 8 and 9 illustrate the influence of rib angle (45°, 60°, 75°, and 90°), rib height ratio (h/H=0–0.6), and rib number (N = 1, 2, 4) on the Nusselt number, friction factor, and Performance Evaluation Criterion (PEC) under turbulent flow conditions. At Re = 5000, the Nusselt number increases strongly with rib height across all angles and rib counts. For the most intensive configuration (N=4, 90° ribs, h/H=0.5), Nu reaches ~56–58, more than double the laminar maximum. Even shallow ribs (h/H=0.1) at 45° provide significant enhancement over a smooth channel. Increasing rib angle further intensifies mixing and flow separation, thus raising Nu, with the 75° and 90° cases showing the steepest growth.

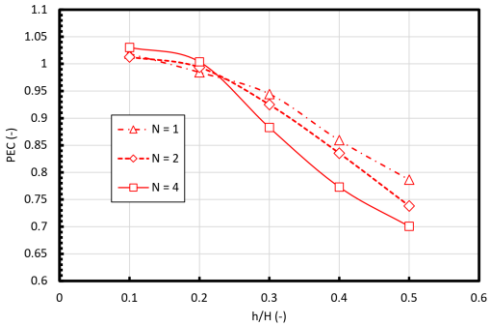

Angle = 45°

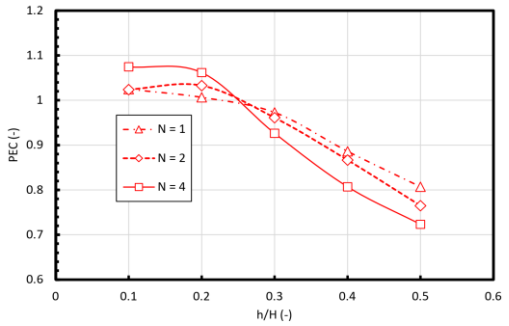

Angle = 60°

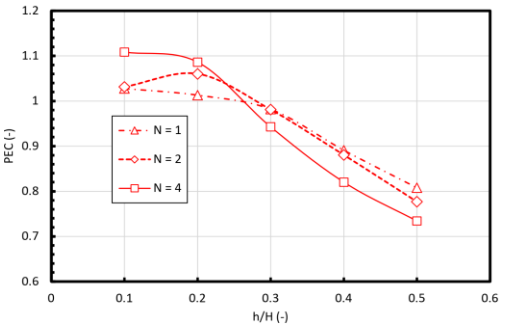

Angle = 75°

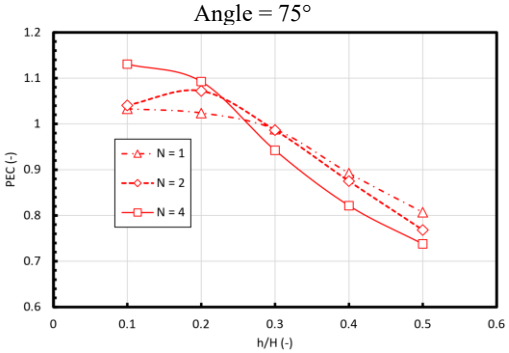

Angle = 90°

Figure 7. Performance Evaluation Criterion (PEC) as a function of h/H for for different rib inclination angles at laminar flow

TABLE 1. Recommended Rib Geometries for Laminar Flow (Re = 500)

Number of Ribs (N)	Recommended Angle (°)	Optimal Height Ratio (h/H)	Design Note
1	45–60	0.2–0.4	High efficiency with minimal pressure penalty
2	~60	0.3–0.4	Balanced trade-off between heat transfer and loss
4	≤ 60 (avoid ≥75)	≤ 0.2	Strong heat transfer but high pressure drop

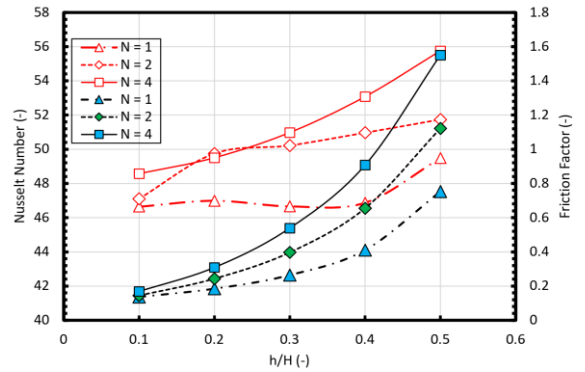

Angle = 45°

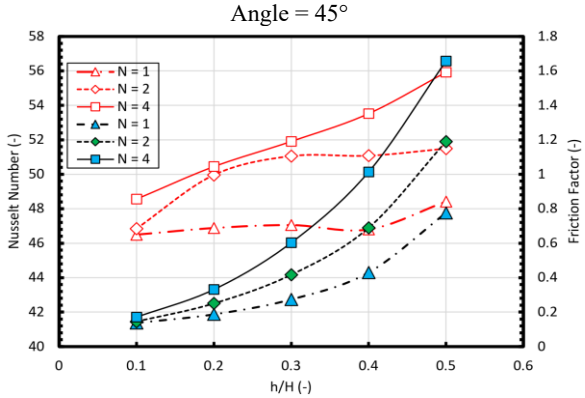

Angle = 60°

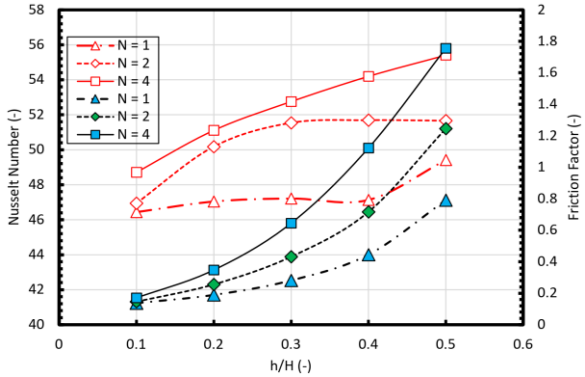

Angle = 75°

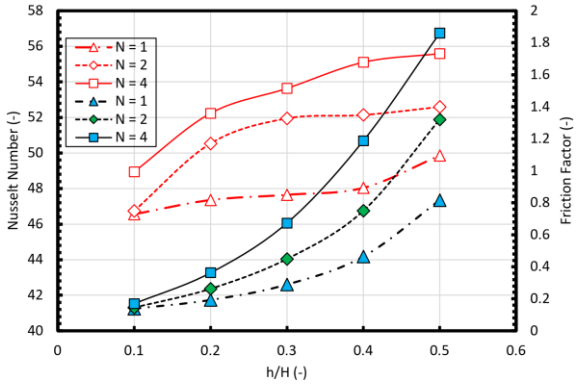

Angle = 90°

Figure 8. Variation of Nusselt number and friction factor as functions of the relative rib height h/H for different rib inclination angles at turbulent flow

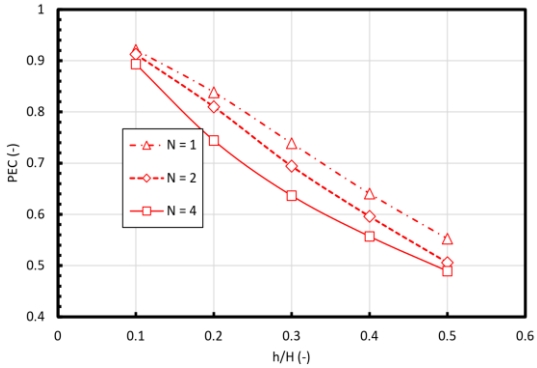

Angle = 45°

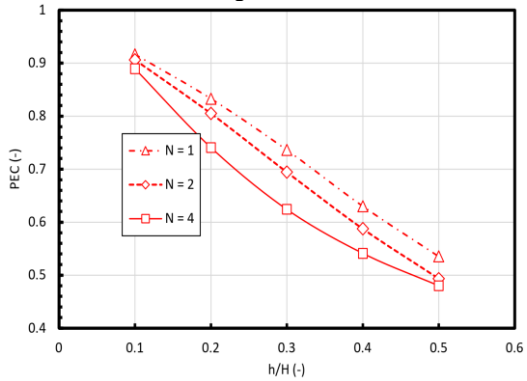

Angle = 60°

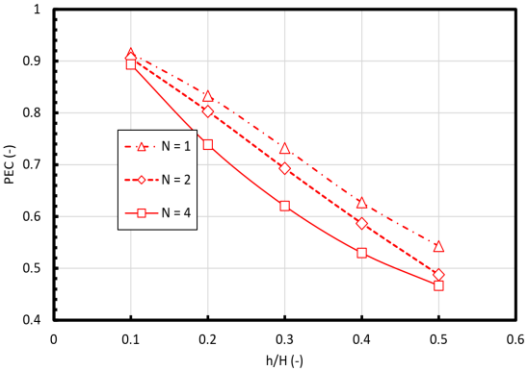

Angle = 75°

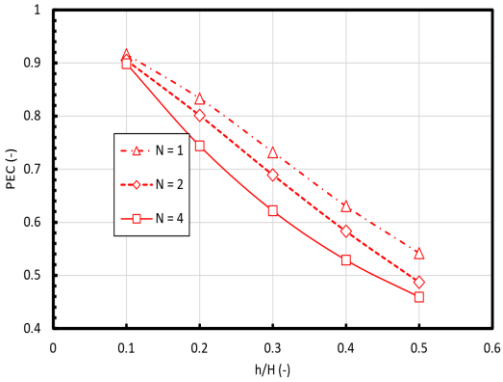

Angle = 90°

Figure 9. Performance Evaluation Criterion (PEC) as a function of h/H for for different rib inclination angles at turbulent flow

The friction factor grows monotonically with rib height and rib density. However, its absolute values are generally lower than in the laminar regime: for instance, at h/H=0.5, f is ~1.5–1.8 for N=4 in turbulence, compared with ~2.5–3.0 in laminar flow. This difference arises because inertial forces dominate turbulent transport, reducing the relative importance of viscous drag. The PEC trends reveal that despite high heat transfer enhancement, overall efficiency declines with rib height. For N=1 at 45°, PEC values remain close to unity for small heights (h/H≤0.2), but they drop rapidly to ~0.5 at h/H=0.5 when N=4. Steeper angles (≥75°) accelerate this decline, as pressure losses rise faster than the thermal benefits.

When comparing the laminar (Re=500) and turbulent (Re=5000) regimes, several key differences emerge in thermal–hydraulic behavior. In laminar flow, ribbed channels provide a modest increase in heat transfer, with the Nusselt number rising to about 21–24 at high rib heights, while friction factors can exceed 2.5–3.0 for dense ribbing. Importantly, under moderate rib heights (h/H=0.2–0.4) and shallow to intermediate rib angles (45°-60°), the PEC approaches or slightly exceeds unity, indicating that a net efficiency gain can be realized. In contrast, turbulent flow delivers a much stronger heat transfer enhancement, with Nusselt numbers reaching 56–58 for high ribs, but this improvement is accompanied by significant hydraulic penalties. Although absolute friction factor values are somewhat lower in turbulence than in laminar flow, the relative energy cost becomes more severe, and as a result, PEC values remain below unity in most configurations, except at very small rib heights and low rib counts. Increasing rib angle consistently boosts heat transfer in both regimes but reduces overall performance efficiency, with the decline more pronounced under turbulence. Overall, while laminar flow offers the possibility of achieving both heat transfer enhancement and acceptable efficiency, turbulent flow emphasizes maximum heat transfer at the expense of efficiency, making careful geometric optimization essential.

5. CONCLUSION

This study investigated the influence of rib angle, rib height, and rib density on the thermal–hydraulic performance of wavy channels under both laminar (Re=500) and turbulent (Re=5000) flow conditions. The results provide several key insights into the interplay between heat transfer enhancement and hydraulic losses:

1. Laminar flow (Re = 500). Ribbed channels produced moderate heat transfer improvements, with Nusselt numbers increasing up to ~24. Friction penalties were relatively high, yet the performance factor (PEC) could approach or slightly exceed unity for optimized geometries, particularly with one or two ribs, moderate rib heights (h/H=0.2–0.4), and rib angles between 45° and 60°. Thus, laminar configurations allow simultaneous improvement in heat transfer and overall efficiency if rib geometry is carefully selected.
2. Turbulent flow (Re = 5000). Heat transfer enhancement was far more pronounced, with Nusselt numbers reaching 56–58 at high rib heights. However, the associated pressure losses intensified, resulting in PEC values that generally remained below unity. Only small rib heights (h/H≤0.2) with a single rib and shallow angles (45°–60°) provided near-balanced performance. Steeper rib angles (≥75°) and higher rib densities yielded maximum Nusselt numbers but at the cost of severe efficiency degradation.
3. Comparison of regimes. Laminar flows present opportunities for balanced design, where both efficiency and heat transfer can be optimized simultaneously. In contrast, turbulent flows favor maximum heat transfer but rarely achieve net thermal-hydraulic efficiency, underscoring the importance of prioritizing either performance or energy economy depending on application requirements.

Acknowledgements

The author appreciates Babol Noshirvani University of Technology for providing necessary facilities to conduct present research.

Funding

No funding was received for conducting this study.

Ethics Approval and Consent to Participate

This article does not involve any studies with human participants or animals performed by any of the authors. Therefore, ethics approval and consent to participate are not applicable.

Competing Interests

The authors declare no financial or organizational conflicts of interest.

Data Availability

The datasets generated during and/or analyzed during the current study are available from the corresponding author on reasonable request.

Declaration of Generative AI and AI-assisted Technologies in the Writing Process

The authors declare that did not use the AI for

generating of any data of this research. All simulations and analyses were performed by the authors, and they bear full responsibility for the content of the publication.

Authors Biosketches

A. Hussein Ghalta: Conceptualization, Methodology, Software, Validation, Formal analysis, Investigation, Data curation, Visualization, Writing—original draft.
M. Farhadi (MF): Conceptualization, Supervision, Project administration, Resources, Writing—review & editing. (Corresponding author.)

REFERENCES

1. Nasiri Khamesloo F, Domiri Ganji D. Optimizing heat transfer in microchannel heat sinks: A numerical investigation with nanofluids and modified geometries. International Journal of Engineering Transactions B: Applications, 2024; 37(5): 860-75. https://doi.org/10.5829/ije.2024.37.05b.05
2. Babaei MR, Sheikhzadeh GA, Abbasian Arani AA. Numerical investigation of geometric parameters effects on heat transfer enhancement in a manifold microchannel heat sink. International Journal of Engineering Transactions B: Applications, 2022; 35(5): 943-53. https://doi.org/10.5829/ije.2022.35.05b.10
3. Safikhani H, Shaabani H. Numerical simulation of frost formation in interrupted microchannel heat sinks considering microfluidic effects in slip regime. International Journal of Engineering Transactions C: Aspects, 2020; 33(12): 2556-62. https://doi.org/10.5829/ije.2020.33.12c.17
4. Sui Y, Lee PS, Teo CJ. An experimental study of flow friction and heat transfer in wavy microchannels with rectangular cross section. International Journal of Thermal Sciences, 2011; 50(12): 2473-82. https://doi.org/10.1016/j.ijthermalsci.2011.06.017
5. Zhou J, Hatami M, Song D, Jing D. Design of microchannel heat sink with wavy channel and its time-efficient optimization with combined RSM and FVM methods. International Journal of Heat and Mass Transfer, 2016; 103: 715-24. https://doi.org/10.1016/j.ijheatmasstransfer.2016.07.100
6. Kaewchoothong N, Maliwan K, Takeishi K, Nuntadusit C. Effect of inclined ribs on heat transfer coefficient in stationary square channel. Theoretical and Applied Mechanics Letters, 2017; 7(6): 344-50. https://doi.org/10.1016/j.taml.2017.09.013
7. Lin L, Zhao J, Lu G, Wang XD, Yan WM. Heat transfer enhancement in microchannel heat sink by wavy channel with changing wavelength/amplitude. International Journal of Thermal Sciences, 2017; 118: 423-34. https://doi.org/10.1016/j.ijthermalsci.2017.05.013
8. Roy R, Kundu B. Effects of fin shapes on heat transfer in microchannel heat sinks. Heat Transfer-Asian Research, 2018; 47(4): 646-59. https://doi.org/10.1002/htj.21332
9. Wang R, Wang J, Lijin B, Zhu Z. Parameterization investigation on the microchannel heat sink with slant rectangular ribs by numerical simulation. Applied Thermal Engineering, 2018; 133: 428-38. https://doi.org/10.1016/j.applthermaleng.2018.01.021
10. Chai L, Wang L. Thermal-hydraulic performance of interrupted microchannel heat sinks with different rib geometries in transverse microchambers. International Journal of Thermal Sciences, 2018; 127: 201-12. https://doi.org/10.1016/j.ijthermalsci.2018.01.029
11. Bahiraei M, Jamshidmofid M, Goodarzi M. Efficacy of a hybrid nanofluid in a new microchannel heat sink equipped with both secondary channels and ribs. Journal of Molecular Liquids, 2019; 273: 88-98. https://doi.org/10.1016/j.molliq.2018.10.003
12. Qidwai MO, Hasan MM. Effect of variation of cylindrical pin fins height on the overall performance of microchannel heat sink. Proceedings of the Institution of Mechanical Engineers, Part E: Journal of Process Mechanical Engineering, 2019; 233(5): 980-90. https://doi.org/10.1177/0954408918821777
13. Zhu JF, Li XY, Wang SL, Yang YR, Wang XD. Performance comparison of wavy microchannel heat sinks with wavy bottom rib and side rib designs. International Journal of Thermal Sciences, 2019; 146: 106068. https://doi.org/10.1016/j.ijthermalsci.2019.106068
14. Li XY, Wang SL, Wang XD, Wang TH. Selected porous-ribs design for performance improvement in double-layered microchannel heat sinks. International Journal of Thermal Sciences, 2019; 137: 616-26. https://doi.org/10.1016/j.ijthermalsci.2018.12.029
15. Wang SL, Chen LY, Zhang BX, Yang YR, Wang XD. A new design of double-layered microchannel heat sinks with wavy microchannels and porous-ribs. Journal of Thermal Analysis and Calorimetry, 2020; 141(1): 547-58. https://doi.org/10.1007/s10973-020-09317-3
16. Wang CS, Wei TC, Shen PY, Liou TM. Lattice Boltzmann study of flow pulsation on heat transfer augmentation in a louvered microchannel heat sink. International Journal of Heat and Mass Transfer, 2020; 148: 119139. https://doi.org/10.1016/j.ijheatmasstransfer.2019.119139
17. Krishna M, Deepu M, Shine SR. Effect of relative waviness on low Re wavy microchannel flow. Journal of The Institution of Engineers (India): Series C, 2020; 101(4): 661-70. https://doi.org/10.1007/s40032-020-00575-6
18. Ahmad EZ, Fazlizan A, Jarimi H, Sopian K, Ibrahim A. Enhanced heat dissipation of truncated multi-level fin heat sink in natural convection for photovoltaic cooling. Case Studies in Thermal Engineering, 2021; 28: 101578. https://doi.org/10.1016/j.csite.2021.101578
19. Khan MN, Karimi MN. Analysis of heat transfer enhancement in microchannel by varying the height of pin fins at upstream and downstream region. Proceedings of the Institution of Mechanical Engineers, Part E: Journal of Process Mechanical Engineering, 2021; 235(4): 758-67. https://doi.org/10.1177/0954408921992975
20. Alsabery AI, Hajjar A, Sheremet MA, Ghalambaz M, Hashim I. Impact of particles tracking model of nanofluid on forced convection heat transfer within a wavy horizontal channel. International Communications in Heat and Mass Transfer, 2021; 122: 105176. https://doi.org/10.1016/j.icheatmasstransfer.2021.105176
21. Zhang YD, Chen MR, Wu JH, Hung KS, Wang CC. Performance improvement of a double-layer microchannel heat sink via novel fin geometry: A numerical study. Energies, 2021; 14(12): 3585. https://doi.org/10.3390/en14123585
22. Khan MZU et al. Investigation of heat transfer in wavy and dual wavy micro-channel heat sink using alumina nanoparticles. Case Studies in Thermal Engineering, 2021; 28: 101515. https://doi.org/10.1016/j.csite.2021.101515
23. Ghorbani N, Targhi MZ, Heyhat MM, Alihosseini Y. Investigation of wavy microchannel ability on electronic devices cooling with the case study of choosing the most efficient microchannel pattern. Scientific Reports, 2022; 12(1): 5882. https://doi.org/10.1038/s41598-022-09859-6
24. Wang S, Zhu J, An D, Zhang B, Chen L, Yang Y, Zheng S, Wang X. Heat transfer enhancement of symmetric and parallel wavy microchannel heat sinks with secondary branch design.

International Journal of Thermal Sciences, 2022; 171: 107229. https://doi.org/10.1016/j.ijthermalsci.2021.107229

25. Okab AK, Hasan HM, Hamzah M, Egab K, Al-Manea A, Yusaf T. Analysis of heat transfer and fluid flow in a microchannel heat sink with sidewall dimples and fillet profile. International Journal of Thermofluids, 2022; 15: 100192. https://doi.org/10.1016/j.ijft.2022.100192
26. Alnaimat F, Varghese D, Mathew B. Investigation of thermal and hydraulic performance of MEMS heat sinks with zig-zag microchannels. International Journal of Thermofluids, 2022; 16: 100213. https://doi.org/10.1016/j.ijft.2022.100213
27. Halon S, Krolicki Z, Revellin R, Zajaczkowski B. Local flow patterns distribution during flow boiling in a micro channel array. Experimental Thermal and Fluid Science, 2023; 141: 110792. https://doi.org/10.1016/j.expthermflusci.2022.110792
28. Fu Y, Liu X, Wang J. Optimal design of wavy microchannel heat sinks based on prediction and multi-objective optimization algorithm. Energy and AI, 2023; 14: 100260. https://doi.org/10.1016/j.egyai.2023.100260
29. Chen CH, Yaji K. Topology optimization for microchannel heat sinks with nanofluids using an Eulerian-Eulerian approach. International Journal of Heat and Mass Transfer, 2025; 98(3): 1125-40. https://doi.org/10.1016/j.ijheatmasstransfer.2025.1125
30. Nasiri Khamesloo F, Domiri Ganji D. Numerical investigation of fractal microchannel heat sinks with modified fin geometries. Iranian Journal of Energy and Environment, 2025; 16(2): 115-25. https://doi.org/10.5829/ijee.2025.16.02.03
31. Nasiri Khamesloo F, Domiri Ganji D. Optimizing heat dissipation in microchannel heat sinks using hybrid nanofluids: A computational study. ResearchGate Preprint, 2024.
32. Zhu J, Li Y, Chen Q. Performance comparison of microchannel heat sinks with various rib shapes and cavities. International Journal of Thermal Sciences, 2024; 192: 108259. https://doi.org/10.1016/j.ijthermalsci.2024.108259
33. Li X, Wang M, Zhang T. Optimizing finned microchannel heat sink design for enhanced thermal performance. Applied Thermal Engineering, 2024; 241: 122426. https://doi.org/10.1016/j.applthermaleng.2024.122426
34. Li Y, Zhao Q, Chen J, Wang L. Optimization of microchannel structures using artificial neural networks and genetic algorithms. Nano Convergence, 2024; 11(1): 20. https://doi.org/10.1007/s42114-024-01002-5
35. Huo Y, Sun Q. Hierarchical embedded microchannel heat sink for ultra-high heat flux SiC chip cooling. arXiv Preprint, 2025; arXiv:2502.18117.
36. Chej M, Pashaei M, Vahdati M. Heat transfer modeling in microfluidic heat sinks with variable thermophysical properties. arXiv Preprint, 2024; arXiv:2402.09931.
37. Al-Bahrani R, Kamari A, Heidari S. Additive manufacturing of topology-optimized heat sinks: A review. Heat Transfer Engineering, 2025; 46(1): 17-35. https://doi.org/10.1080/01457632.2025.2459981
38. Jalilinasrabady S, Hashemnia A, Kalantari M. Performance analysis of inclined microchannel-incorporated heat sinks for electronics cooling. Journal of Enhanced Heat Transfer, 2025; 32(3): 231-44.
39. Dehkordi AR, Farhadi M, Akbari M. Optimization of sinusoidal and Z-shaped microchannels for improved cooling performance. International Communications in Heat and Mass Transfer, 2024; 147: 107573. https://doi.org/10.1016/j.icheatmasstransfer.2024.107573
40. Mousavi F, Rahimi M. Effect of varying cross-sectional microchannel designs on heat sink performance. Experimental Thermal and Fluid Science, 2024; 141: 110851. https://doi.org/10.1016/j.expthermflusci.2024.110851
41. Ghasemi M, Arasteh AA. Thermal analysis of fluted-fin microchannels in laminar flows. Energy Conversion and Management, 2024; 284: 117128. https://doi.org/10.1016/j.enconman.2023.117128
42. Alimohammadi H, Jamshidi N. Investigation of Y-shaped bifurcated microchannels for thermal management applications. Applied Thermal Engineering, 2024; 243: 122735. https://doi.org/10.1016/j.applthermaleng.2024.122735
43. Liu H, Shi X. Triangular lattice network design for uniform heat distribution in microchannel heat sinks. Thermal Science and Engineering Progress, 2025; 30: 101301. https://doi.org/10.1016/j.tsep.2025.101301
44. Lu B, Jiang PX. Experimental and numerical investigation of convection heat transfer in a rectangular channel with angled ribs. Experimental Thermal and Fluid Science, 2005; 30(6): 513-21. https://doi.org/10.1016/j.expthermflusci.2005.09.007

Persian Abstract

چکیده

این مطالعه به بررسی عملکرد حرارتی–هیدرولیکی کانال‌های موج‌دار مجهز به ریب‌های عرضی می‌پردازد و به نیاز به راهکارهای بهینه‌سازی انتقال حرارت در مبدل‌های حرارتی فشرده پاسخ می‌دهد؛ جایی که اثرات ترکیبی هندسه ریب و رژیم جریان به‌طور کافی مورد مطالعه قرار نگرفته‌اند. هدف این تحقیق، ارزیابی تأثیر زاویه شیب، ارتفاع، و تعداد ریب‌ها بر بهبود انتقال حرارت و کارایی کلی، در شرایط جریان آرام (Re = 500) و آشفته (Re = 5000) است. شبیه‌سازی‌های عددی سه‌بعدی با استفاده از نرم‌افزار ANSYS Fluent برای تحلیل ویژگی‌های انتقال حرارت، افت فشار و معیار ارزیابی عملکرد (PEC) انجام شده‌اند. نتایج نشان می‌دهند که ریب‌های عرضی با ایجاد جدایش جریان و تشکیل گردابه‌ها، به‌طور چشمگیری انتقال حرارت را افزایش می‌دهند. در جریان آرام، عدد ناسلت تا حدود ۵۰٪ نسبت به کانال صاف افزایش یافت، به‌ویژه در ریب‌هایی با ارتفاع متوسط(h/H = 0.2–0.4) ، زاویه ٤٥ تا ٦٠ درجه و تعداد کم (N = 1–2) که مقدار PEC بهینه نیز حاصل شد. در جریان آشفته، افزایش انتقال حرارت محسوس‌تر بود (عدد ناسلت حدود ٥٦ تا ٥٨)، اما اصطکاک بیشتر منجر به کاهش مقدار PEC به کمتر از یک در اکثر موارد شد. در این تحقیق، تعادل‌های نوینی شناسایی شد که بین عملکرد حرارتی و کارایی کلی تعادل ایجاد می‌کنند، به‌ویژه در شرایط جریان آرام. این یافته‌ها دستورالعمل‌های طراحی ارزشمندی را برای بهینه‌سازی هندسی کانال‌های موج‌دار دارای ریب در رژیم‌های مختلف جریان ارائه می‌دهند.